ACS NANO
Cite This: ACS Nano 2018, 12, 6137–6146
www.acsnano.org

ARTICLE

MapZ Forms a Stable Ring Structure That Acts As a Nanotrack for FtsZ Treadmilling in *Streptococcus mutans*

Yongliang Li,[†] Shipeng Shao,[‡] Xiao Xu,[†] Xiaodong Su,[§] Yujie Sun,*[,‡] and Shicheng Wei*[,†]

[†]Department of Oral and Maxillofacial Surgery/Central Laboratory, School and Hospital of Stomatology, Peking University, National Engineering Laboratory for Digital and Material Technology of Stomatology, 22 Zhonguancun South Road, Haidian District, Beijing 100081, China

[‡]State Key Laboratory of Membrane Biology, Biodynamic Optical Imaging Center (BIOPIC), School of Life Sciences, Peking University, 5 Yiheyuan Road, Beijing 100871, China

[§]Biodynamic Optical Imaging Center (BIOPIC), School of Life Sciences, Peking University, Beijing 100871, China

Supporting Information

ABSTRACT: **Bacterial binary cell division requires accurate placement of division machinery. FtsZ, a vital component of the division machinery, can assemble into filaments and self-organize into a ring structure (Z ring) at the appropriate site for cell division. MapZ, a recently identified FtsZ regulator in *Streptococcaceae*, has been found to localize at the midcell where it helps to properly position the FtsZ ring. However, its mechanism is still unclear. Here, by using total internal reflection fluorescence microscopy, super-resolution imaging, and single molecule tracking, we investigated the mechanism by which MapZ controls the position of the FtsZ ring. Our results show that FtsZ exhibits a dynamic treadmilling motion in *S. mutans*. Importantly, depletion of MapZ leads to the unconstrained movement of treadmilling FtsZ filaments and a shorter lifetime of the constricting FtsZ ring, which is frequently misplaced. Furthermore, by revealing that MapZ forms an immobile ring-like nanostructure at the division site, our study suggests that MapZ forms a stable ring that acts as a nanotrack to guide and restrict treadmilling FtsZ filaments in *S. mutans*.**

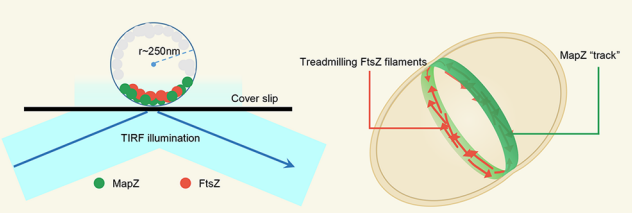

KEYWORDS: *cell division, FtsZ treadmilling, MapZ, single molecule tracking, super-resolution imaging, Streptococcus*

In bacteria, the eukaryotic tubulin homologue FtsZ[1] is a core component of cell division machinery. Upon initiation of cell division, FtsZ proteins self-organize into a heterogeneous ring nanostructure (Z ring) at the site of cell division[2] where they recruit other proteins involved in division.[3] Many studies have investigated the regulatory mechanisms that controls the positioning and timing of Z ring formation. In well-studied model bacteria, such as *Escherichia coli* and *Bacillus subtilis*, the Min system[4] and the Nucleoid Occlusion (NO) system[5] have been identified as two important negative regulatory systems, which prevent Z ring assembly in inappropriate locations by inhibiting FtsZ polymerization.[6,7] MipZ is another negative regulator of FtsZ; it was discovered in *Caulobacter crescentus* and is conserved among the *Alphaproteobacteria*. MipZ directly interacts with FtsZ and alters the formation of FtsZ filaments to prevent inappropriate Z-ring formation.[8] Distinct from the negative regulatory systems mentioned above, several positive control systems have also been reported. For example, an SsgA/SsgB-mediated system was identified in *Streptomyces*,[9] and a PomZ-mediated system was identified in *Myxococcus xanthus*.[9,10] These systems do not affect the position of Z ring formation through inhibition of FtsZ polymerization. Instead, these proteins congregate at the site of cell division, prior to the arrival of FtsZ, where they regulate Z ring formation.

Recently, another important regulatory system was discovered in *Streptococcus pneumoniae* and found to be conserved in other *Streptococcaceae*, which lacks both of the aforementioned FtsZ regulatory components. This system is mediated by the transmembrane protein MapZ (also called LocZ),[11,12] which is a substrate of the Ser/Thr kinase StkP[13] (also called PknB in *S. mutans*[14,15]). MapZ binds to peptidoglycan *via* its extracellular domain[11,16] and positions the Z ring through a direct interaction between its cytoplasmic domain and FtsZ. In the absence of MapZ, the FtsZ ring mislocalizes at the midcell and displays an aberrant plane angle.[11,17] In contrast with other

Received: April 3, 2018
Accepted: May 29, 2018
Published: May 29, 2018

DOI: 10.1021/acsnano.8b02469
ACS Nano 2018, 12, 6137–6146

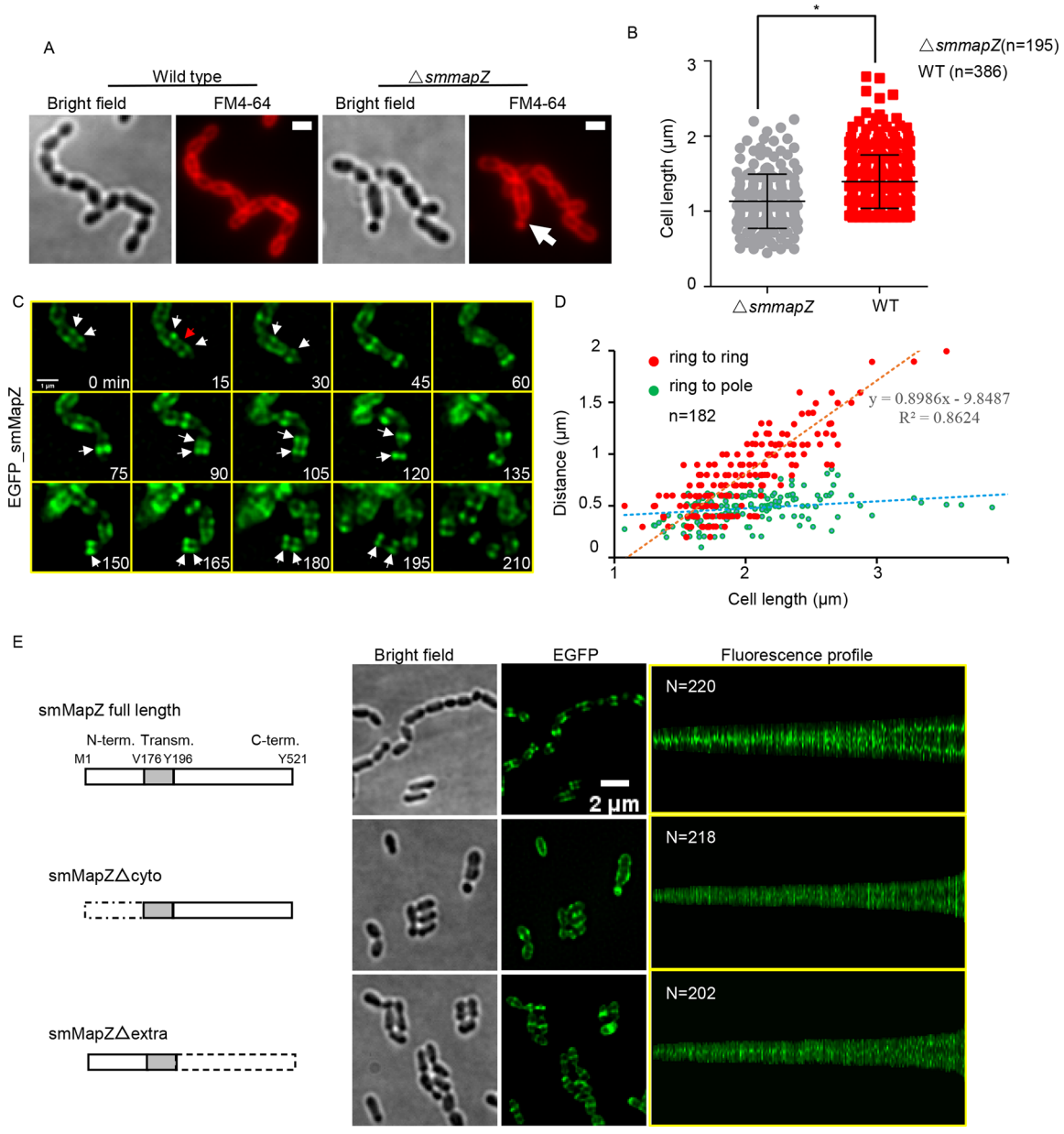

Figure 1. Characterization of a MapZ homologue in *S. mutans* (smMapZ). (A) The representative images of cell shape of wild type (WT) and *smmapZ* deletion mutant (Δ*smmapZ*). FM4-64 (red) was used to stain the cell membrane. A minicell is indicated by the white arrow. Scale bar, 1 μm. (B) Distribution of cell length of WT (386 cells) and Δ*smmapZ* (195 cells). A statistical analysis was performed using the Mann−Whitney U test. '*' indicates $P < 0.05$. (C) Snapshots of fluorescence time-lapse imaging of strain EGFP_smMapZ. EGFP_smMapZ was expressed at the native locus under the control of its native promoter. White arrows indicate the split smMapZ rings, and the red arrow indicates a third smMapZ ring. (D) Distance between the two outer smMapZ rings (red dots) and between the smMapZ rings and the nearest pole (green dots). 182 cells harboring more than two smMapZ rings were analyzed using the Microbetracker and custom Matlab codes (see Materials and Methods). The linear fitted curve and R^2 value for the distance between the two smMapZ rings are shown. (E) Localization pattern of full length smMapZ, smMapZ with cytoplasmic domain deletion (smMapZΔcyto), and the extracellular domain null mutation (smMapZΔextra). A schematic picture of mutation construction (left), representative bright field images and EGFP fluorescence images (middle), and corresponding maps of the integrated fluorescence profiles (right) are shown. The fluorescence intensity of each cell (Y axis) is ordered by the cell length which is increasing from the left to right (X axis). *N* indicates the number of analyzed cells.

FtsZ regulators, such as MinC, SimA, MipC, and SsgB, which directly affect FtsZ polymerization,[6−8,10] MapZ does not display an obvious influence on FtsZ polymerization or its GTPase activity.[11] This suggests that MapZ regulates the Z ring position in a way that has not been previously reported. Despite the important role of MapZ, few studies have investigated its mechanism of action.

FtsZ also self-organizes into filaments, which exhibit a dynamic treadmilling action *in vitro*.[18] Recently, this dynamic treadmilling was experimentally confirmed in model bacteria, *E. coli* and *B. subtilis*.[19,20] The treadmilling of FtsZ filaments drives cell wall synthesis, which is a crucial step in septum formation and cell division. To gain more insight into how MapZ regulates the Z ring position, we studied the influence of MapZ on FtsZ treadmilling. Here, we show that MapZ plays an

DOI: 10.1021/acsnano.8b02469
ACS Nano 2018, 12, 6137−6146

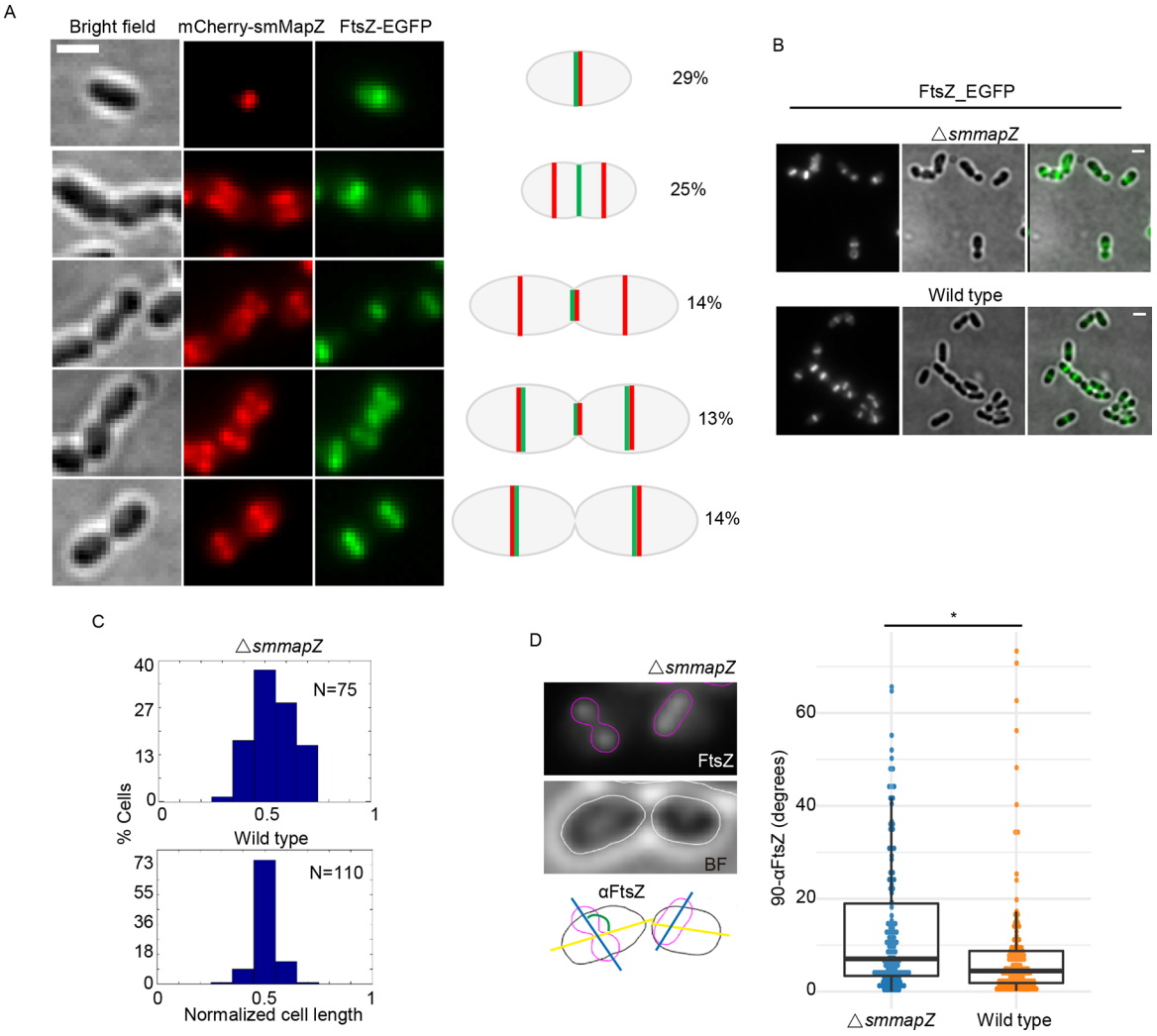

Figure 2. Influence of smMapZ on FtsZ position. (A) Localization relationship between smMapZ and FtsZ. Cells, in which smMapZ was labeled with mCherry (red) and FtsZ was labeled with EGFP, were analyzed using fluorescence microscopy. The cartoons (with corresponding cell ratios) on the right depict the position of smMapZ and FtsZ rings. In total, 213 cells were analyzed. Scale bar, 1 μm. (B) Representative images of FtsZ rings in WT and Δ*smmapZ* cells. Cells expressing FtsZ_EGFP were analyzed by fluorescence microscopy. Scale bar, 1 μm. (C) Distribution of the FtsZ ring position in WT and Δ*smmapZ* cells; 0.5 represents the middle position in a cell. 75 and 110 cells were analyzed using MicrobeTracker and custom Matlab code (see Materials and Methods). (D) Distribution of the Z ring plane angle in WT and Δ*smmapZ* strains. The Z ring plane angle (*α*FtsZ) was analyzed using Oufti and R scripts to measure the angle between the long axis of Z ring outlines and the long axis of cell outlines. The Z ring (top, purple outline), cell (middle, white outline), and schematic diagram of *α*FtsZ (bottom) are shown on the left. The 90° - *α*FtsZ angle was plotted with median value. '*' represents $P < 0.05$ (Mann−Whitney U test). 130 cells each of the WT and Δ*smmapZ* strains were selected and measured.

integral role in cell shape and Z ring localization during cell division in *S. mutans*. MapZ controls the positioning and plane angle of the Z ring by guiding the orientation and positioning of FtsZ filaments that undergo treadmilling. Furthermore, we used super-resolution imaging and single molecule tracking to discover that MapZ forms a stable and heterogeneous ring-like nanostructure at the site of cell division, acting as a track to guide and restrict the position of treadmilling FtsZ filaments to form a proper Z ring. Our study sheds light on the mechanism by which MapZ controls the FtsZ ring position in *Streptococcaceae*. Importantly, it also provides insight into bacterial regulation of cell division.

RESULTS AND DISCUSSION

Here, to gain an understanding of how MapZ controls the position of the FtsZ ring during bacterial cell division, we studied the MapZ homologue in *S. mutans* (called smMapZ henceforth), an important Gram-positive pathogen that can be easily cultured and genetically modified.[21] smMapZ shows only 37% sequence identity with MapZ in *S. pneumoniae* (spMapZ), with 32% and 50% sequence identity for the cytoplasmic and extracellular domains, respectively. This low sequence identity is consistent with the poorly conserved amino acid sequence of spMapZ in *Enterococcaceae* and *Streptococcaceae*,[22] which showed that the average sequence identity of the spMapZ cytoplasmic domain and the extracellular domain is 28.4% and 59.5%, respectively, in *Enterococcaceae* and *Streptococcaceae*.

Most of the first 40 amino acids of spMapZ, which are sufficient for the interaction of spMapZ and FtsZ, are absent in smMapZ. However, two phosphorylation sites (T67 and T78)[11,12] and several amino acids (R409, Y411, N428, Y430, Y450, F451, and N454)[16] required for binding to pneumococcal peptidoglycan are conserved (Figure S1A). Analysis of

DOI: 10.1021/acsnano.8b02469
ACS Nano 2018, 12, 6137−6146

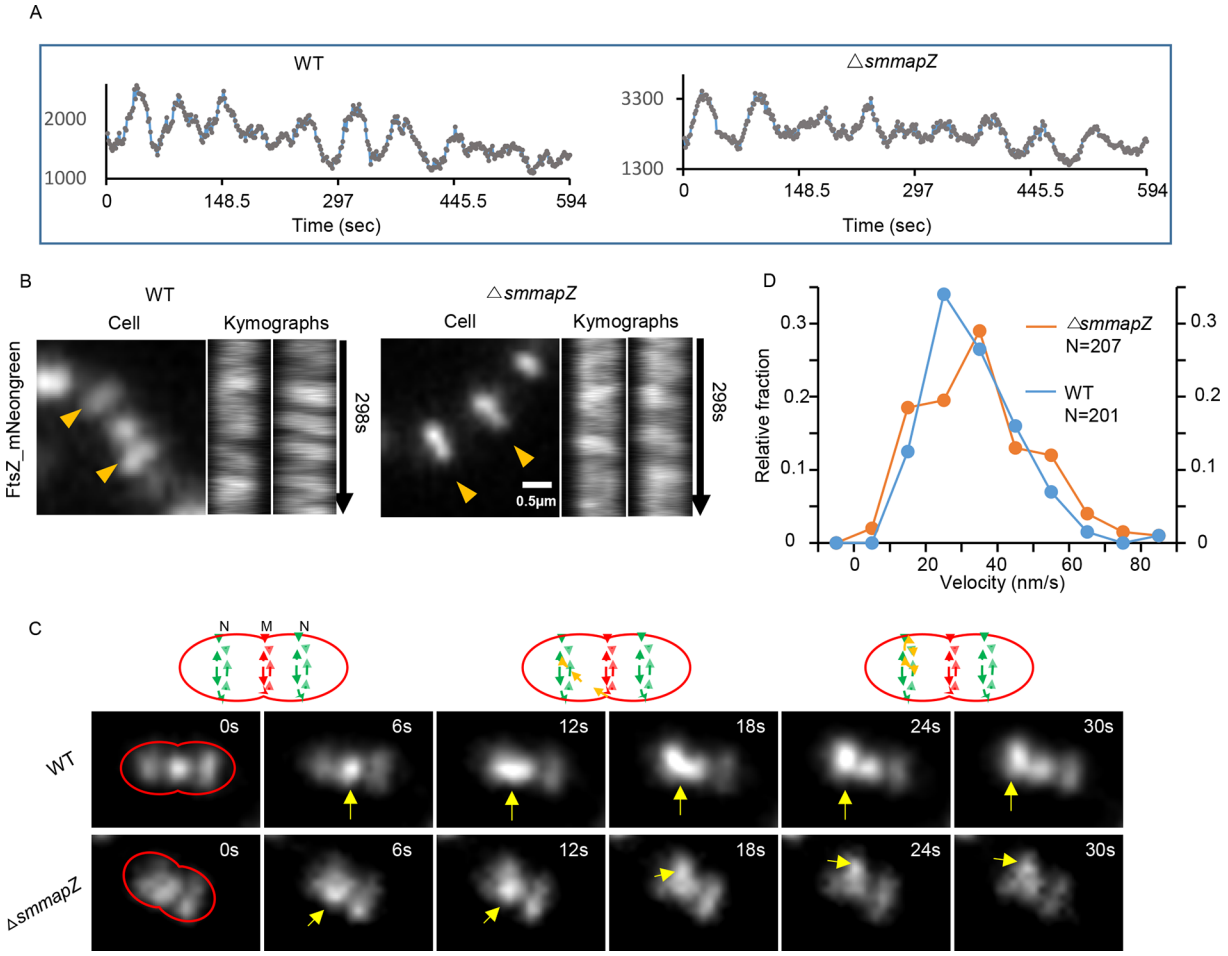

Figure 3. FtsZ shows directional movement independent of smMapZ. (A) Representative fluorescence intensity time traces of FtsZ rings in WT and Δ*smmapZ* strains. (B) The use of FtsZ_mNeongreen reveals directional movement of FtsZ rings in WT and Δ*smmapZ* strains (1 frames/1.5 s, Movies s1 and s2). The kymographs show the movement of FtsZ filaments inside the Z rings (orange arrows). (C) Translocation of FtsZ filaments in WT and Δ*smmapZ* cells (1 frames/1.5 s, Movies s3 and s4). Schematics are shown above. "M" refers to the middle (original) ring, and "N" refers to newly formed rings. Fluorescence images are shown below. The red outline indicates cell shape, and yellow arrows mark the FtsZ filaments undergoing translocation. (D) Distribution of the velocity of FtsZ filaments movement inside the Z rings of WT and Δ*smmapZ* cells. 201 and 207 motion events were analyzed for WT and Δ*smmapZ*, respectively.

amino acid conservation (Figure S1B), prediction of sequence disorder tendency (Figure S1C), and prediction of secondary structure elements of the intracellular domain (Figure S1D) suggested that smMapZ folds into a structure potentially similar to spMapZ, with a cytoplasmic domain containing a predicted functional subdomain at the N-terminus and an extracellular domain composed of two subdomains.

smMapZ is essential for normal cell shape formation. Deletion of the *mapZ* gene in *S. mutans* (Δ*smmapZ*) led to shorter, irregularly shaped cells and mini-cells (Figure 1A, B); this mutation phenotype is similar to that in *S. pneumoniae*. To test whether this phenotype resulted from a polar effect due to smMapZ depletion, we complemented ectopically expressed smMapZ under the control of the xylose-inducable P_{ldh} promoter in the Δ*smmapZ* strain (named Δ*smmapZ*/P_{ldh}-smMapZ). Culturing this strain in the absence of xylose led to the formation of short cells and minicells, which is similar to the phenotype of the Δ*smmapZ* strain (Figure S2A). When grown in the presence of xylose (10 mg/mL), the cells showed a similar morphology and cell size compared to the WT strain (Figure S2).

To assess the localization pattern of smMapZ, we fused enhanced green fluorescent protein (EGFP) to the N-terminus of smMapZ under the control of the native promoter (Figure S3). Time-lapse imaging of EGFP-smMapZ (Figure 1C) indicated that smMapZ formed a ring at the midcell, and a pair of rings appeared as the cell elongated. The distance between the two smMapZ rings increased as a function of cell length, while the distance between the smMapZ rings and their nearest cell pole did not change obviously (Figure 1D), suggesting that the smMapZ ring at the midcell split into two rings, which remain anchored at the cell equator of the new daughter cells. Interestingly, both the cytoplasmic domain and the extracellular domain are required for the septal localization of smMapZ. smMapZ with a cytoplasmic domain deletion (*smmapZΔcyto*) resulted in loss of the ability to position the rings at the constricting septum, differing from that of spMapZ.[11] Most of the extracellular domain null mutation (*smmapZΔextra*) diffused on the membrane, but part of the smMapZΔextra still retained a septum localization pattern (Figure 1E), which is consistent with a recent study of spMapZ.[16] Next, to illustrate which domains are responsible for such a particular localization pattern of smMapZ, we

DOI: 10.1021/acsnano.8b02469
ACS Nano 2018, 12, 6137−6146

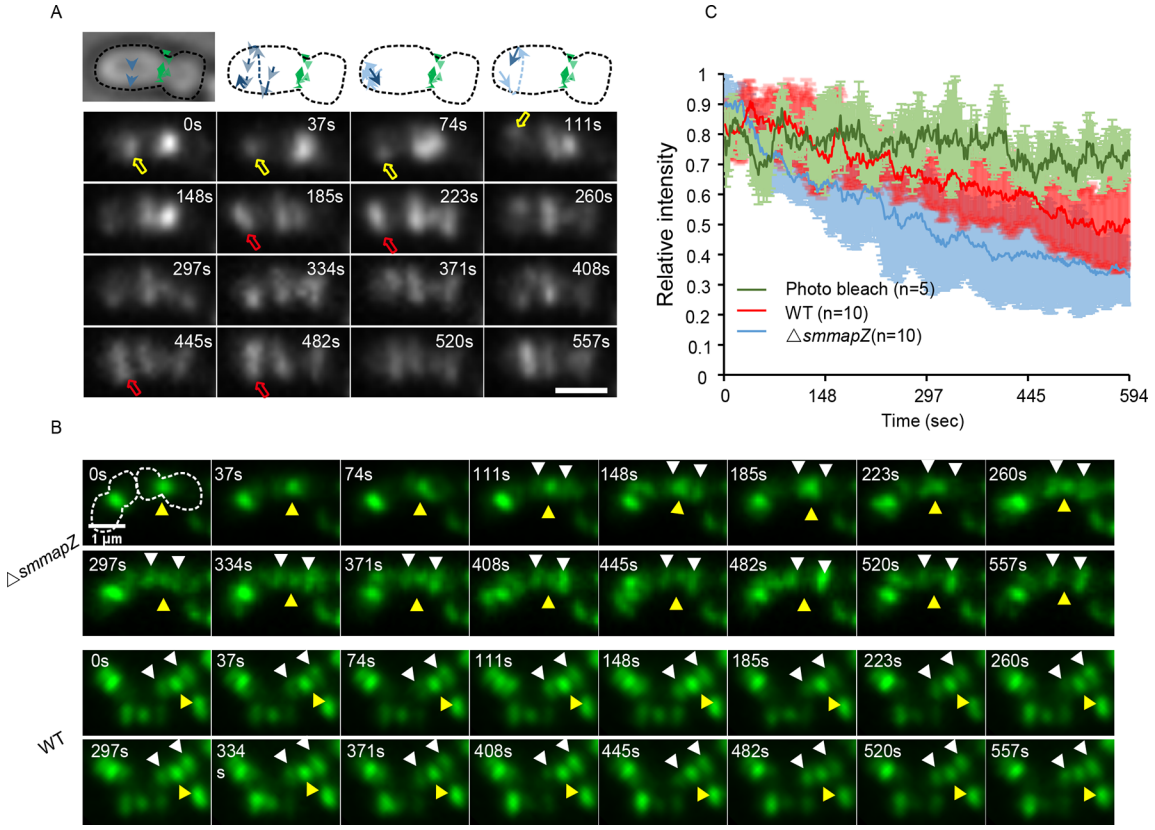

Figure 4. Deletion of *smmapZ* leads to unconstrained FtsZ treadmilling and shorter lifetime of the constricting FtsZ ring. (A) FtsZ_mNeongreen shows unconstrained FtsZ treadmilling in Δ*smmapZ* cells (1 frames/1.5 s, Movie s5). Cartoons (top) demonstrate the motion of FtsZ filaments during the first 100 s of cell division. Dotted lines mark cell outlines based on bright field images (upper left). Dark blue arrows indicate the position and direction of FtsZ filament movement. Light blue arrows indicate the movement paths of the filaments. Yellow arrows in the time-lapse snapshots (bottom four rows) mark the position of FtsZ filaments, and red arrows indicate changes in the FtsZ ring plane. Scale bar, 1 μm. (B) Time-lapse snapshots of Three-FtsZ-Ring structures in Δ*smmapZ* and WT cells (Movies s7 and s8). White arrows mark the positions of newly formed FtsZ rings, and yellow arrows mark the positions of the middle (original) FtsZ rings. (C) Fluorescence intensity time traces of the middle (original) FtsZ ring in WT and Δ*smmapZ* cells. 10, 10, and 5 intensity time traces of Z-rings were averaged resulting in curves for WT, Δ*smmapZ*, and photobleach, respectively. Five Z rings without obvious motion (checked visually) were selected to measure the photobleach.

constructed six strains expressing differently truncated smMapZ (Figure S4). We found that deletion of the unconserved subdomains of the cytoplasmic domain (T4) led to impaired ability of smMapZ to position at the septum. Deletion of a subdomain tandem to the transmembrane region of the extracellular domain (T5) resulted in septum localization of smMapZ, while deletion of the C-terminal subdomain of the extracellular domain (T6) led to diffuse localization of smMapZ, similar to that reported in the recent study.[16] Further, we performed an evolutionary tree analysis which revealed that smMapZ and spMapZ belong to different evolutionary branches (Figure S5), in line with the domain function analysis, suggesting that *S. mutans* might use a different mechanism for smMapZ localization at the septum. The sequence analysis and characterization of smMapZ suggest a similar structure and localization pattern of smMapZ and spMapZ.

To determine whether smMapZ, like spMapZ, is important for FtsZ positioning, we next studied the localization relationship between the FtsZ ring and the smMapZ ring. In newly divided wild type cells, FtsZ and smMapZ colocalized at the midcell. As cells grew, the initial smMapZ ring split into a pair of rings, each ring remaining associated with the equator of one of the daughter cells and being thus localized at the division site before the FtsZ ring (Figure 2A). Moreover, smMapZ was required for correct localization of the FtsZ ring, as 64% of FtsZ rings were unable to localize at the midcell in the Δ*smmapZ* strain, while only 22.7% of FtsZ rings mislocalized in the wild-type (WT) strain (Figure 2B, C). To gain more insight into the role of smMapZ in regulating the Z ring plane, we measured the angle of the FtsZ ring relative to the cell's long axis (*α*FtsZ) in the WT and Δ*smmapZ* strains. The results showed that the FtsZ ring is more skewed in the Δ*smmapZ* strain. The median value of 90° - *α*FtsZ was 7.05 ± 1.329 in the Δ*smmapZ* strain, while it was 4.44 ± 1.13 in the WT strain (Figure 2D). These results are consistent with previous reports.[11,12,17]

As a tubulin homologue in prokaryotic cells, the treadmilling motion of FtsZ filaments was confirmed *in vivo* recently.[19,20] MapZ did not affect the polymerization and GTPase activity of FtsZ,[11] but deletion of MapZ did impact FtsZ ring localization and constriction. Thus, we proposed that MapZ might control the treadmilling of FtsZ filaments. To test this hypothesis, we labeled FtsZ with a brighter green fluorescent protein (mNeongreen) and used TIRFM to study the dynamics of FtsZ rings. The results revealed a periodic fluctuation in intensity of the FtsZ ring (Figure 3A, Figure S6A). Using kymograph, we observed directional movement of the FtsZ ring (Figure 3B, Movie s1) similar to that observed in *E. coli* and *B.*

DOI: 10.1021/acsnano.8b02469
ACS Nano 2018, 12, 6137–6146

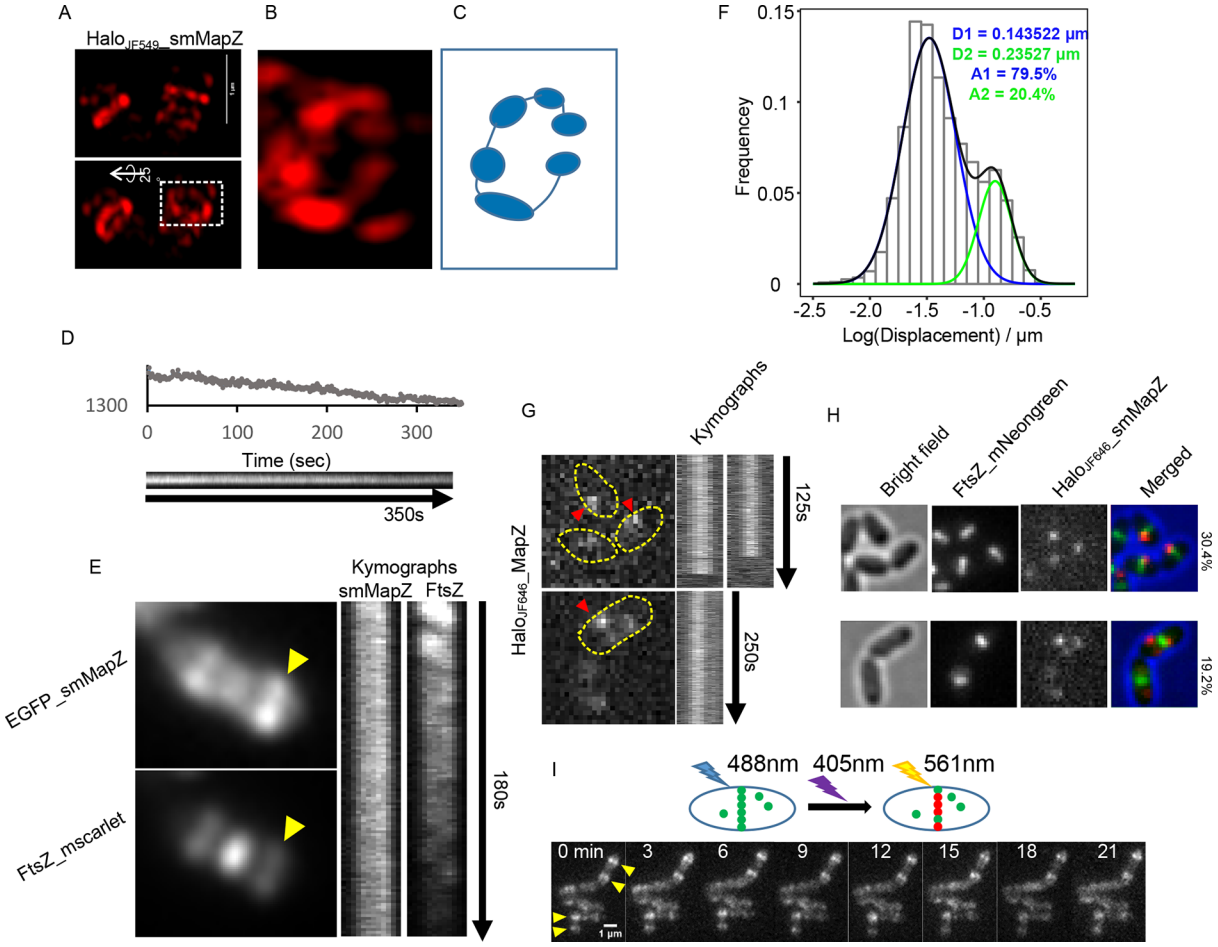

Figure 5. Characterization of the smMapZ ring. (A) Three-dimensional structured illumination microscopy (3D-SIM) image of HaloJF$_{549}$_smMapZ (15 min incubation with 500 nm JF$_{549}$ dye, Movie s9). Z projection view (top) and rotated view (25° around the *x*-axis, bottom) are shown. Scale bar, 1 μm. (B) Enlarged boxed region in (A) shows the heterogeneous structure of the smMapZ ring. (C) Cartoon of the heterogeneous ring structure shown in (B). (D) Representative fluorescence intensity time trace and kymograph of mNeongreen_smMapZ (1 frame/s, Movie s10). (E) The strain, expressing EGFP_smMapZ and FtsZ_mScaret-I, was analyzed by TIRF microscopy. Kymographs show the intensity change inside the smMapZ ring and FtsZ rings (yellow arrows). (F) Distribution of log(Displacement) of single molecule tracking of smMapZ (15 min incubation with 62.5pM JF$_{646}$ dye). The Gaussian fitting curve (blue, green, black), the average Displacement (D1 and D2), and the area of the two populations are shown. (G) HaloJF$_{646}$_smMapZ shows stationary molecules. Dotted curves indicate cell outlines, with kymographs drawn from the positions of the red arrows. (H) The localization relationship (with corresponding cell ratios) between the stationary smMapZ molecules and FtsZ_mNeongreen in the newborn (upper) and the grown (lower) cells. 125 cells selected based on bright field images were analyzed. (I) Time-lapse snapshots of mMaple3_smMapZ collected by TIRF microscopy. The cartoon shows that a 405 nm laser transforms the partial mMaple3 to the red form, which was then excited by a 561 nm laser. smMapZ ring structures are marked by yellow arrows.

subtilis,[19,20] indicating that the treadmilling behavior of FtsZ filaments is conserved in different bacterial species. In contrast with *E. coli*, in which only one FtsZ ring forms during a cell cycle, three FtsZ rings forming dumbbell structures could be observed in the majority of *S. mutans* and *S. pneumoniae*[11,12] cells at a later stage in the cell cycle. Surprisingly, during cell division, we observed translocation of FtsZ filaments from the original FtsZ ring to a new FtsZ ring forming nearby (six such events were observed among 83 cells harboring the Three-FtsZ-Ring structure) (Figure 3C, Movie s3); this has not been reported in other bacterial species. Considering that the speed of FtsZ filament translocation was similar to the speed of treadmilling inside the ring and that translocated FtsZ filaments participate in new ring formation, it is reasonable to conclude that FtsZ translocation is a functional process rather than an abnormal one. The treadmilling movement of FtsZ filaments around the Z ring and translocation of FtsZ filaments may explain the heterogeneous structure of Z rings in *S. pneumoniae* observed with 3D-SIM and PLAM.[23−27]

Interestingly, deletion of the *smmapZ* gene led to highly unconstrained movement of FtsZ filaments (Figure 4A, Movies s5 and s6), but did not perturb the treadmilling and translocation of FtsZ filaments (Figure 3A-C, Movies s2 and s4) or alter the speed of treadmilling (Figure 3D). This suggests a crucial role for smMapZ in guiding the treadmilling movement of FtsZ filaments. Although the unconstrained FtsZ filaments could still form a ring-like structure as the cell grew, the angle of the FtsZ ring plane changed back and forth during FtsZ ring formation, which might ultimately lead to aberrant localization of the Z ring (Figures 4A, S6B), in line with a recent report in *S. pneumoniae*.[11,17] Nevertheless, once a Z ring has formed, the Z ring plane angle can no longer change (Figure S6C, Movie s5). These results may explain why

DOI: 10.1021/acsnano.8b02469
ACS Nano 2018, 12, 6137−6146

depletion of smMapZ leads to an irregular cell shape and minicell formation.

Consistent with previous research,[11] we also noticed that deletion of *smmapZ* resulted in a decrease in the frequency of observations of cells with three FtsZ rings (Figure S6D). By monitoring the complete process of emergence and disappearance of the Three-FtsZ-Ring structure, we discovered that the middle FtsZ ring in the Δ*smmapZ* strain only remained 5−6 min after new FtsZ ring formation, exhibiting a shorter lifetime than in the WT strain (>10 min) (Figure 4B, Movies s7 and s8). Analysis of the FtsZ ring intensity trace also indicated that deleting *smmapZ* led to a more rapid decrease in fluorescence of the middle FtsZ ring than in WT (Figure 4C). We speculate that the shorter lifetime was caused by an increase in FtsZ translocation (Movie s5) in absence of the restricting and guiding role of smMapZ; however, we cannot exclude the possibility that it may have been due to premature constriction of the FtsZ ring, as previously described.[11]

Next, to understand how smMapZ guides the treadmilling of FtsZ filaments, we performed three-dimensional structured illumination microscopy (3D-SIM) to study the nanostructure of a Halotag-fused smMapZ ($Halo_{JF549}$-smMapZ[28]) ring. The smMapZ ring exhibited a heterogeneous ring-like nanostructure like spMapZ as well[11] at the division site (Figure 5A-C, Movie s9), similar to previously identified nanostructures of FtsZ, EzrA, Pbp2,[24] FtsA, and ZipA.[26] Such discontinuous ring nanostructures allow for direct observation of their directional movements using single molecule TIRF imaging.[19,20] Here, to study the dynamic movements of the smMapZ ring, we labeled smMapZ with mNeongreen for TIRF imaging. Interestingly, no obviousperiodic motion of smMapZ was observed by intensity time traces or kymograph analysis (Figure 5D, Figure S7A, Movie s10). A cell shape and growth curve analysis excluded the possibility of dysfunction of smMapZ due to the mNeongreen label (Figure S8). These results suggest that the smMapZ ring is immobile. We further observed the relative movement of smMapZ and FtsZ using a dual color assay. By labeling smMapZ and FtsZ with EGFP and mScarlet-I,[29] respectively, we revealed that the FtsZ ring exhibited directional movement while the smMapZ ring showed no obvious movement (Figure 5E).

Single molecule tracking allowed us to measure the spatially specific dynamic features of targeted molecules. Here, we labeled Halotag-fused smMapZ with low concentrations (62.5 pM) of HaloLigand-JF_{646} to monitor the motion of single smMapZ molecules. The results revealed two populations of smMapZ molecules: (i) stationary and (ii) diffusive (Figure 5F, Movie s11). In a few cases, we also observed that a single smMapZ molecule switched between the two modes (Figure S7B). We analyzed the localization pattern of stationary smMapZ molecules in 62 cells. In 38 cells that exhibited newly divided cell length or Three-FtsZ-Ring structures, the stationary smMapZ molecules colocalized with the FtsZ ring. In the other 24 cells, the stationary smMapZ molecules localized at the cell equators of the future daughter cells (Figure 5G, H, Figure S7C). The low mobility of smMapZ molecules supports the hypothesis that smMapZ forms a stable ring structure. However, as most single molecules were bleached in 1−3 min, single molecule trajectories were insufficient for studying the stability of the smMapZ ring over a longer period of time. Therefore, we labeled smMapZ with mMaple3, a photoconvertible fluorescent protein which converts from green fluorescence to red fluorescence under purple illumination.[30] Using TIRF illumination, we photoconverted mMaple3-fused smMapZ molecules in the bottom portion of the ring using a 405 nm laser and monitored their movement every 3 min. The results showed that over a total duration of 21 min, neither the position nor the intensity of the photoconverted smMapZ molecules changed obviously, indicating that the smMapZ ring is a stable structure and the exchange of smMapZ molecules occurs at a very slow rate (Figure 5I, Figure S7D). We therefore propose a mechanism in which a stable smMapZ ring structure serves as a "track" during cell division, which guides dynamic treadmilling FtsZ filaments to the proper position where they organize into a Z ring (Figure 6). Our work suggests an interesting mechanism that bacteria control Z ring formation by guiding the positioning and orientation of FtsZ filaments undergoing treadmilling.

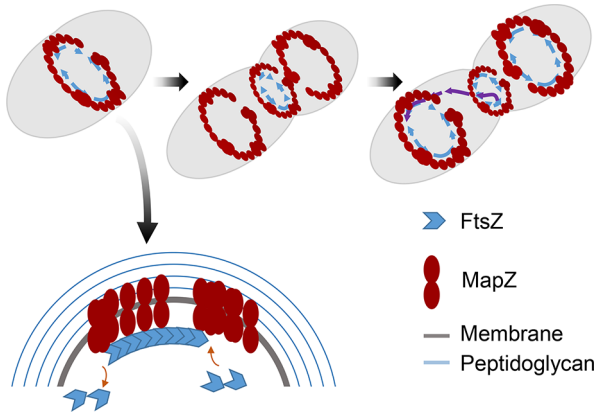

Figure 6. Model for smMapZ guides treadmilling FtsZ filaments in *S. mutans*. smMapZ forms a stable heterogeneous ring-like structure at the site of cell division. The stable ring acts as a track for treadmilling FtsZ filaments, and, as the cell grows, this stable smMapZ ring migrates to the future cell division sites in daughter cells before formation of the Z ring. Newly formed FtsZ filaments will move along the stable smMapZ ring, and the translocated FtsZ filaments will participate in the formation of a new Z ring.

CONCLUSIONS

A transmembrane MapZ-mediated FtsZ regulatory system discovered in *S. pneumoniae* is known to be conserved in *Streptococcaceae*.[11] However, it is unclear how MapZ controls the position of FtsZ proteins and, hence, Z ring formation. Here, our data suggest that a MapZ homologue in *S. mutans* forms a stable heterogeneous ring-like nanostructure at site of cell division, which may act as guiding track for treadmilling FtsZ filaments (Figure 6). Nevertheless, in spite of its essential role in guiding the position and angle of the FtsZ ring, smMapZ is not required for FtsZ ring formation. Our data reveal that changes in the FtsZ ring plane angle often occurred early during its formation, but not during constriction. Thus, we propose that smMapZ functions as a track for FtsZ filaments only during the early stages of FtsZ ring formation. Other proteins may be involved in stabilizing the position and orientation of the FtsZ ring plane after Z ring formation, such as EZrA, a spectrin-like protein,[31] which has been reported to interact with FtsZ and is required for correct localization of the FtsZ ring.[32] Considering the similar functions of smMapZ and spMapZ, we propose that the "track" model of smMapZ does not only exist in *S. mutans*, but also in other MapZ-conserved

DOI: 10.1021/acsnano.8b02469
ACS Nano 2018, 12, 6137−6146

bacteria. Previous studies[11,17] showing that spMapZ plays a role in setting the correct angle of the Z-ring are consistent with our study.

Recently, two studies focused on the question of what regulates MapZ at the division site. Manuse et al. revealed a two-subdomain structure of the extracellular domain, indicating that the two subdomains may permit structural rearrangement of MapZ and regulate its binding to peptidoglycan.[16] Van Raaphorst et al. showed that the position of the origin of chromosome replication instead of MapZ is crucial for division site selection in *S. pneumoniae*.[17]

Our study complements these studies by shedding light on the mechanism by which MapZ regulates the position of the FtsZ ring and provides a greater understanding of the MapZ-mediated FtsZ regulatory system. However, in addition to the "track" role of the MapZ ring, it may also serve as a "road fence" to restrict and guide FtsZ treadmilling. In order to distinguish these two possibilities, a better understanding of the interaction between MapZ and FtsZ is required in future.

MATERIALS AND METHODS

Bacterial Strains, Plasmid and Mutation Construction, and Culture Conditions. *S. mutans* standard strain UA159 and all derived strains used in this study are listed in Table S1. To generate *S. mutans* mutations (gene deletion, gene knock in, and fluorescent protein fusion), we used a counter-selectable system called IFDC2 (provided by Zhoujie Xie). Bacterial transformation was performed as previously described.[33] Briefly, an overnight culture grown in Todd−Hewitt medium supplemented with 0.3% yeast extract (THY; QinDao Wei Si, China) was diluted (1:20) in the same medium and incubated for 2−3 h (OD_{600} 0.2−0.3). Five μL of SOE PCR reaction and 0.5 μL of CSP (1 μg/μL stock) were added to 500 μL of culture and incubated for 2 h. To select antibiotic-resistant colonies, brain heart infusion (BHI; Difco Laboratories, Detroit, MI, USA) agar plates were supplemented with 12 μg/mL erythromycin (Sigma-Aldrich, St. Louis, MO, USA). Selection of the second transformation was performed on BHI plates supplemented with 4 mg/mL p-cl-Phe (Sigma-Aldrich). For snapshot imaging, *S. mutans* strains were aerobically cultured in THY at 37 °C. For time-lapse imaging, the strains were cultured in a chemically defined medium[34] supplemented with 0.3% yeast extract (C + Y). A final concentration of 10 mg/mL xylose was added to the culture medium to induce the expression of pZX9 and pZX10[35] (provided by Jiezhou Xie).

Sample Preparation for Snapshot Imaging. An overnight culture grown in THY medium was diluted (1:100) in the same medium and incubated at 37 °C under aerobic conditions to OD_{600} 0.4−0.5 (7 h). The culture was diluted again (1:100) and grown under the same conditions to OD_{600} 0.1−0.2 (5 h). Cells were harvested by centrifugation at 1,500 × *g* for 3 min, washed three times with 1× phosphate-buffered saline (PBS), and resuspended in 1× PBS. The bacteria were loaded between a gel pad (1× PBS supplemented with 1.5% low-melting agarose) and a coverslip (Fisher 24× 50, No. 1.5). For FtsZ imaging, spectinomycin was added to all cultures at a final concentration of 1 mg/mL. D (+) xylose (Sigma-Aldrich) was added before the last round of dilution at 10 mg/mL.

Sample Preparation for 3D-SIM Imaging. JF_{549} dye (500 nM; provided by Luke Lavis) was added to the culture at OD_{600} 0.1−0.2, incubated for 15 min at 37 °C, washed once with 1× PBS, fixed in 4% paraformaldehyde for 15 min at room temperature, and washed twice with 1× PBS. Resuspended cells were loaded between the coverslip (Fisher 24 × 50, No. 1.5) and the gel pad.

Sample Preparation for Time-Lapse Imaging. *EGFP_smMapZ and mMaple3_smMapZ.* An overnight culture grown in THY medium was diluted (1:100) in C + Y medium. After two dilutions, the culture at OD_{600} 0.1−0.2 was added to a gel pad (C + Y medium supplemented with 1.5% low-melting agarose) on a glass slide; a coverslip was then placed on top of the gel pad. Rectangular 3 M double-sided tape was used to seal the coverslip and glass slide.

$HaloJF_{646}$_smMapZ. JF_{646} dye (62.5 pM) was added to the culture at OD_{600} 0.1−0.2. The culture was incubated for 15 min at 37 °C and washed once with prewarmed fresh C + Y medium. Resuspended cells were loaded between the coverslip and the gel pad.

Imaging of FtsZ_mNeongreen. Spectinomycin was added to all cultures at a final concentration of 1 mg/mL. D (+) xylose was added at 10 mg/mL before the last round of dilution.

Slide Preparation. Coverslips (Fisherbrand, Fisher scientific) were cleaned with Piranha solution (30% H_2O_2: 98% H_2SO_4 v:v = 1:3 at 90 °C for 30 min), rinsed and stored in Milli-Q water, and dried with high purity nitrogen before use.

Snapshot Imaging of smMapZ and FtsZ. Bacterial samples were visualized on an N-STORM (Nikon, Tokyo, Japan) system equipped with a 100× oil TIRF objective lens (Nikon PLAN APO, 1.49 NA), Andor-897 EMCCD (Andor, Belfast, Northern Ireland), the perfect focus system (Nikon), a laser source (405, 488, 561, and 647 nm), and 1.5× magnification optics. Images were collected with Nis-Elements AR software (Nikon). For EGFP_smMapZ and mCherry_smMapZ, 300 frames were collected with a 100 ms exposure time. For FtsZ_EGFP, 50 frames were collected with a 100 ms exposure time.

Time-Lapse Imaging of EGFP_smMapZ and mMaple3_smMapZ. Time-lapse observation of EGFP_smMapZ was performed with a DeltaVision OMX SR (GE Healthcare, Little Chalfont, UK) system equipped with a 1.42 NA 60× oil objective (Olympus, Tokyo, Japan), laser source (405, 488, 561, and 642 nm), four sCOMS, and an environmental control system. Using OMX Acquisition software, images were collected with a 60 ms exposure time at 5 min intervals at a constant temperature of 37 °C.

Time-lapse imaging of mMaple3_smMapZ was collected by TIRF illumination on an N-STORM microscope equipped with a live cell instrument. A laser at 405 nm was used to photoconvert the mMaple3 to the red form with an initial exposure time of 300 ms. Then, a 561 nm laser with a 400 ms exposure time was used to excite the red state mMaple3, and a 488 nm laser with a 300 ms exposure time was used to excite the green state.

3D-SIM Imaging of $HaloJF_{549}$_smMapZ. Super-resolution 3D-SIM imaging was performed using a DeltaVision OMX SR system with a 10 ms exposure time and 50% transmission. The 3D-SIM raw data were reconstructed with SoftWoRx 6.0 (Applied Precision, Issaquah, WA, USA) using a Wiener filter setting of 0.001 and a channel that specifically measured optical transfer functions. The immersion oil was optimized to 1.518.

Imaging the Dynamics of FtsZ_mNeongreen, Dual Color Labeled Strain, mNeongreen_smMapZ, and HaloJF646_smMapZ. Images were collected by near-TIRF illumination on an N-STORM microscope. mNeongreen and EGFP were excited by the 488 nm laser, while mScarlet-I was excited by the 561 nm laser. The 647 nm laser was used to excite the JF646 dye. For FtsZ_mNeongreen, exposure time was 0.165 s, interval time was 0.495 s, and the images were collected at room temperature. For the single molecular track of HaloJF646-smMapZ, exposure time was 0.1 s, and the interval time was 0.5 s. For mNeongreen_smMapZ, exposure time was 0.5 s, and the interval time was 0.5 s. For EGFP_smMapZ and FtsZ_mScarlet-I dual color labeled strain, exposure time was 0.5 s, and interval time was 0.5 s.

Data Analysis. The raw.nd2 image stacks obtained by Nis-Elements AR software were transformed to .tiff files, and ImageJ software (NIH, Bethesda, MD, USA) was used to carry out Z-projections. The images were further processed in MicrobeTracker[36] to extract information on cell outline and fluorescence signals. Cell outlines were detected manually based on bright field images. The data were further processed using custom Matlab codes (https://github.com/interestinghua/MapZ-and-FtsZ-rings/tree/master) to identify the peak of the integrated fluorescence signal profile; its position was determined to be the site of smMapZ ring and FtsZ ring localization.

Information regarding the cell length of WT and ΔsmMapZ was extracted, and a graph was generated using Microsoft Excel software (Microsoft Corp., Redmond, WA, USA).

DOI: 10.1021/acsnano.8b02469
ACS Nano 2018, 12, 6137−6146

To compare the distance between the two outer smMapZ rings and between the smMapZ ring and the cell pole, the information regarding the cell length and fluorescence signals of EGFP_smMapZ strain was analyzed using the custom code 'Extract information and Distance'. Cells with only one ring structure were excluded before the data were analyzed, and the graph was generated in Excel.

To sort the fluorescence intensity of the smMapZ truncations as a function of cell length, deconvolution was performed on averaged images using Huygens software, and the images were subsequently analyzed using Coli-Inspector in the ImageJ plugin ObjectJ (http://simon.bio.uva.nl/objectj/), as previously described.[16] Cells were selected manually based on the bright field images.

The angle of the Z ring plane in WT and Δ*smmapZ* cells was determined as previously described.[17] Briefly, the cell outline was manually detected with Oufti's cell detection tool, and the Z ring was detected with an object detection tool. The data was further analyzed using R scripts "ouftimeshtransform", "Polygon_angle", and "angles and length" to determine αFtsZ (the angle between the long axis of the Z ring outline and the long axis of the cell outline), and the results were plotted.

We used Fiji (http://fiji.sc/) to analyze the periodic intensity fluctuations of the Z ring and treadmilling. First, drift correction of the time-lapse imaging was performed using the Fiji plugin named "Descriptor-based series registration (2d/3d + t)" (developed by Stephan Preibisch). We selected a medium detection brightness and a six-pixel detection size; the type of detection was set as minima and maxima, and the rest were set as default values. After drift correction, a 3 × 3-pixel (~320 nm) region of interest was chosen inside the Z ring, and the *Z*-axis profile was plotted with Fiji to show periodic intensity fluctuations. For analysis of FtsZ treadmilling, the images were resized to 26 nm/pixel using the bicubic method, a segmented line (line width 11) was drawn inside the Z ring parallel to its long axis, and a multiple kymograph plugin was used to demonstrate movement. The velocity of treadmilling was calculated using a kymograph macro called "read velocities from tsp", as described in the detailed plugin description (https://www.embl.de/eamnet/html/body_kymograph.html).

Single Particle Tracking. The Fiji plugin TrackMate[37] (http://imagej.net/TrackMate) was used to analyze the trajectory of single molecules of smMapZ. We selected the LoG detector and set 0.4 μm as the estimated blob diameter. The LAP Tracker function, with a 0.5 μm maximum distance for frame-to-frame linking, was employed to complete the tracking. The trajectory data were exported, and further analysis of log(Displacement) was carried out in R studio (R Development Core Team, Vienna, Austria) using a custom script (https://github.com/interestinghua/MapZ-and-FtsZ-rings/tree/master, log(Displacement) distribution). The two-status analysis of single trajectory was performed in MATLAB using the HMM-Bayes procedure,[38] as previously described.

smMapZ Sequence Analysis. To identify the smMapZ protein, we selected the spMapZ protein sequence as the query sequence and used BLAST (https://blast.ncbi.nlm.nih.gov/Blast.cgi) to search the proteome of *S. mutans*. The smMapZ and spMapZ protein sequences were aligned using SnapGene software (GSL Biotech LLC, Chicago, IL, USA). The smMapZ transmembrane domain was predicted using the TMHMM Server v. 2.0 (http://www.cbs.dtu.dk/services/TMHMM/). Network Protein Sequence Analysis[39] (http://npsa-pbil.ibcp.fr) was used to predict the secondary structure of the smMapZ cytoplasmic domain, as previously described. In total, 150 protein sequences were selected to determine amino acid conservation using the Consurf Web server[40] (http://consurf.tau.ac.il/2016/). Prediction of sequence disordered tendency was performed using IUPred[41] (http://iupred.enzim.hu/).

ASSOCIATED CONTENT

Supporting Information

The Supporting Information is available free of charge on the ACS Publications website at DOI: 10.1021/acsnano.8b02469.

Experimental data and strain list (PDF)

Movie s1, directional movement of FtsZ inside the Z ring in WT cells (AVI)

Movie s2, directional movement of FtsZ inside the Z ring in Δ*smmapZ* cells (AVI)

Movie s3, translocation of FtsZ in WT cells (AVI)

Movie s4, translocation of FtsZ in Δ*smmapZ* cells (AVI)

Movie s5, unconstrained movement of FtsZ in Δ*smmapZ* cells (AVI)

Movie s6, unconstrained movement of FtsZ in Δ*smmapZ* cells (AVI)

Movie s7, lifetime of constricting FtsZ ring in Δ*smmapZ* cells (AVI)

Movie s8, lifetime of constricting FtsZ ring in WT cells (AVI)

Movie s9, ring structure of $Halo_{JF549}$_smMapZ (AVI)

Movie s10, timelapse of mNeongreen_smMapZ in WT cells (AVI)

Movie s11, single molecule tracking of smMapZ (AVI)

AUTHOR INFORMATION

Corresponding Authors

*E-mail: sc-wei@pku.edu.cn.

*E-mail: sun_yujie@pku.edu.cn.

ORCID

Yongliang Li: 0000-0001-5016-2778

Shicheng Wei: 0000-0001-5570-3393

Notes

The authors declare no competing financial interest.

ACKNOWLEDGMENTS

This work was funded by the National Natural Science Foundation of China (Grant nos. 30973317, 31271423, and 21390412) and Peking University's 985 Grant. We thank Zhoujie Xie (Institute of Microbiology, CAS) for his assistance in the construction of the mutations and Chunyan Shan (The Core Imaging Facility of Peking University) for her help on DeltaVision OMX. We thank He Yu, Professor Can Xie, and ShuJin Luo (School of Life Sciences, Peking University) for their help with analysis of the evolutionary tree.

REFERENCES

(1) Lowe, J.; Amos, L. A. Crystal Structure of the Bacterial Cell-Division Protein Ftsz. *Nature* **1998**, *391*, 203−206.

(2) Bi, E. F.; Lutkenhaus, J. Ftsz Ring Structure Associated with Division in Escherichia Coli. *Nature* **1991**, *354*, 161−164.

(3) Adams, D. W.; Errington, J. Bacterial Cell Division: Assembly, Maintenance and Disassembly of the Z Ring. *Nat. Rev. Microbiol.* **2009**, *7*, 642−653.

(4) Rowlett, V. W.; Margolin, W. The Bacterial Min System. *Curr. Biol.* **2013**, *23*, R553−556.

(5) Wu, L. J.; Errington, J. Nucleoid Occlusion and Bacterial Cell Division. *Nat. Rev. Microbiol.* **2012**, *10*, 8−12.

(6) Cho, H.; McManus, H. R.; Dove, S. L.; Bernhardt, T. G. Nucleoid Occlusion Factor Slma Is a DNA-Activated Ftsz Polymerization Antagonist. *Proc. Natl. Acad. Sci. U. S. A.* **2011**, *108*, 3773−3778.

(7) Hu, Z.; Mukherjee, A.; Pichoff, S.; Lutkenhaus, J. The Minc Component of the Division Site Selection System in Escherichia Coli Interacts with Ftsz to Prevent Polymerization. *Proc. Natl. Acad. Sci. U. S. A.* **1999**, *96*, 14819−14824.

(8) Thanbichler, M.; Shapiro, L. Mipz, a Spatial Regulator Coordinating Chromosome Segregation with Cell Division in Caulobacter. *Cell* **2006**, *126*, 147−162.

(9) Treuner-Lange, A.; Aguiluz, K.; van der Does, C.; Gomez-Santos, N.; Harms, A.; Schumacher, D.; Lenz, P.; Hoppert, M.; Kahnt, J.;

DOI: 10.1021/acsnano.8b02469
ACS Nano 2018, 12, 6137−6146

Munoz-Dorado, J.; Sogaard-Andersen, L. Pomz, a Para-Like Protein, Regulates Z-Ring Formation and Cell Division in Myxococcus Xanthus. *Mol. Microbiol.* **2013**, *87*, 235−253.
(10) Willemse, J.; Borst, J. W.; de Waal, E.; Bisseling, T.; van Wezel, G. P. Positive Control of Cell Division: Ftsz Is Recruited by Ssgb During Sporulation of Streptomyces. *Genes Dev.* **2011**, *25*, 89−99.
(11) Fleurie, A.; Lesterlin, C.; Manuse, S.; Zhao, C.; Cluzel, C.; Lavergne, J. P.; Franz-Wachtel, M.; Macek, B.; Combet, C.; Kuru, E.; VanNieuwenhze, M. S.; Brun, Y. V.; Sherratt, D.; Grangeasse, C. Mapz Marks the Division Sites and Positions Ftsz Rings in Streptococcus Pneumoniae. *Nature* **2014**, *516*, 259−262.
(12) Holeckova, N.; Doubravova, L.; Massidda, O.; Molle, V.; Buriankova, K.; Benada, O.; Kofronova, O.; Ulrych, A.; Branny, P. Locz Is a New Cell Division Protein Involved in Proper Septum Placement in Streptococcus Pneumoniae. *mBio* **2015**, *6*, e01700-14−e01700-14.
(13) Manuse, S.; Fleurie, A.; Zucchini, L.; Lesterlin, C.; Grangeasse, C. Role of Eukaryotic-Like Serine/Threonine Kinases in Bacterial Cell Division and Morphogenesis. *FEMS Microbiol. Rev.* **2016**, *40*, 41−56.
(14) Banu, L. D.; Conrads, G.; Rehrauer, H.; Hussain, H.; Allan, E.; van der Ploeg, J. R. The Streptococcus Mutans Serine/Threonine Kinase, Pknb, Regulates Competence Development, Bacteriocin Production, and Cell Wall Metabolism. *Infect. Immun.* **2010**, *78*, 2209−2220.
(15) Hussain, H.; Branny, P.; Allan, E. A Eukaryotic-Type Serine/Threonine Protein Kinase Is Required for Biofilm Formation, Genetic Competence, and Acid Resistance in Streptococcus Mutans. *J. Bacteriol.* **2006**, *188*, 1628−1632.
(16) Manuse, S.; Jean, N. L.; Guinot, M.; Lavergne, J. P.; Laguri, C.; Bougault, C. M.; VanNieuwenhze, M. S.; Grangeasse, C.; Simorre, J. P. Structure-Function Analysis of the Extracellular Domain of the Pneumococcal Cell Division Site Positioning Protein Mapz. *Nat. Commun.* **2016**, *7*, 12071.
(17) van Raaphorst, R.; Kjos, M.; Veening, J. W. Chromosome Segregation Drives Division Site Selection in Streptococcus Pneumoniae. *Proc. Natl. Acad. Sci. U. S. A.* **2017**, *114*, E5959−E5968.
(18) Loose, M.; Mitchison, T. J. The Bacterial Cell Division Proteins Ftsa and Ftsz Self-Organize into Dynamic Cytoskeletal Patterns. *Nat. Cell Biol.* **2014**, *16*, 38−46.
(19) Yang, X.; Lyu, Z.; Miguel, A.; McQuillen, R.; Huang, K. C.; Xiao, J. Gtpase Activity-Coupled Treadmilling of the Bacterial Tubulin Ftsz Organizes Septal Cell Wall Synthesis. *Science* **2017**, *355*, 744−747.
(20) Bisson-Filho, A. W.; Hsu, Y. P.; Squyres, G. R.; Kuru, E.; Wu, F.; Jukes, C.; Sun, Y.; Dekker, C.; Holden, S.; VanNieuwenhze, M. S.; Brun, Y. V.; Garner, E. C. Treadmilling by Ftsz Filaments Drives Peptidoglycan Synthesis and Bacterial Cell Division. *Science* **2017**, *355*, 739−743.
(21) Lemos, J. A.; Quivey, R. G., Jr.; Koo, H.; Abranches, J. Streptococcus Mutans: A New Gram-Positive Paradigm? *Microbiology* **2013**, *159*, 436−445.
(22) Garcia, P. S.; Simorre, J. P.; Brochier-Armanet, C.; Grangeasse, C. Cell Division of Streptococcus Pneumoniae: Think Positive! *Curr. Opin. Microbiol.* **2016**, *34*, 18−23.
(23) Fu, G.; Tao, H.; Buss, J.; Coltharp, C.; Hensel, Z.; Jie, X. *In Vivo* Structure of the E. Coli Ftsz-Ring Revealed by Photoactivated Localization Microscopy (Palm). *PLoS One* **2010**, *5*, e12680.
(24) Strauss, M. P.; Liew, A. T.; Turnbull, L.; Whitchurch, C. B.; Monahan, L. G.; Harry, E. J. 3d-Sim Super Resolution Microscopy Reveals a Bead-Like Arrangement for Ftsz and the Division Machinery: Implications for Triggering Cytokinesis. *PLoS Biol.* **2012**, *10*, e1001389.
(25) Buss, J.; Coltharp, C.; Huang, T.; Pohlmeyer, C.; Wang, S.-C.; Hatem, C.; Xiao, J. *In Vivo* Organization of the Ftsz-Ring by Zapa and Zapb Revealed by Quantitative Super-Resolution Microscopy. *Mol. Microbiol.* **2013**, *89*, 1099−1120.
(26) Rowlett, V. W.; Margolin, W. 3d-Sim Super-Resolution of Ftsz and Its Membrane Tethers in Escherichia Coli Cells. *Biophys. J.* **2014**, *107*, L17−20.
(27) Jacq, M.; Adam, V.; Bourgeois, D.; Moriscot, C.; Di Guilmi, A. M.; Vernet, T.; Morlot, C. Remodeling of the Z-Ring Nanostructure During the Streptococcus Pneumoniae Cell Cycle Revealed by Photoactivated Localization Microscopy. *mBio* **2015**, *6*, e01108-15.
(28) Grimm, J. B.; English, B. P.; Chen, J.; Slaughter, J. P.; Zhang, Z.; Revyakin, A.; Patel, R.; Macklin, J. J.; Normanno, D.; Singer, R. H.; Lionnet, T.; Lavis, L. D. A General Method to Improve Fluorophores for Live-Cell and Single-Molecule Microscopy. *Nat. Methods* **2015**, *12*, 244−250 243 p following 250..
(29) Bindels, D. S.; Haarbosch, L.; van Weeren, L.; Postma, M.; Wiese, K. E.; Mastop, M.; Aumonier, S.; Gotthard, G.; Royant, A.; Hink, M. A.; Gadella, T. W., Jr. Mscarlet: A Bright Monomeric Red Fluorescent Protein for Cellular Imaging. *Nat. Methods* **2017**, *14*, 53−56.
(30) Wang, S.; Moffitt, J. R.; Dempsey, G. T.; Xie, X. S.; Zhuang, X. Characterization and Development of Photoactivatable Fluorescent Proteins for Single-Molecule-Based Superresolution Imaging. *Proc. Natl. Acad. Sci. U. S. A.* **2014**, *111*, 8452−8457.
(31) Cleverley, R. M.; Barrett, J. R.; Basle, A.; Bui, N. K.; Hewitt, L.; Solovyova, A.; Xu, Z. Q.; Daniel, R. A.; Dixon, N. E.; Harry, E. J.; Oakley, A. J.; Vollmer, W.; Lewis, R. J. Structure and Function of a Spectrin-Like Regulator of Bacterial Cytokinesis. *Nat. Commun.* **2014**, *5*, 5421.
(32) Jorge, A. M.; Hoiczyk, E.; Gomes, J. P.; Pinho, M. G. Ezra Contributes to the Regulation of Cell Size in Staphylococcus Aureus. *PLoS One* **2011**, *6*, e27542.
(33) Xie, Z.; Okinaga, T.; Qi, F.; Zhang, Z.; Merritt, J. Cloning-Independent and Counterselectable Markerless Mutagenesis System in Streptococcus Mutans. *Appl. Environ. Microbiol.* **2011**, *77*, 8025−8033.
(34) van de Rijn, I.; Kessler, R. E. Growth Characteristics of Group a Streptococci in a New Chemically Defined Medium. *Infect. Immun.* **1980**, *27*, 444−448.
(35) Xie, Z.; Qi, F.; Merritt, J. Development of a Tunable Wide-Range Gene Induction System Useful for the Study of Streptococcal Toxin-Antitoxin Systems. *Appl. Environ. Microbiol.* **2013**, *79*, 6375−6384.
(36) Sliusarenko, O.; Heinritz, J.; Emonet, T.; Jacobs-Wagner, C. High-Throughput, Subpixel Precision Analysis of Bacterial Morphogenesis and Intracellular Spatio-Temporal Dynamics. *Mol. Microbiol.* **2011**, *80*, 612−627.
(37) Tinevez, J. Y.; Perry, N.; Schindelin, J.; Hoopes, G. M.; Reynolds, G. D.; Laplantine, E.; Bednarek, S. Y.; Shorte, S. L.; Eliceiri, K. W. Trackmate: An Open and Extensible Platform for Single-Particle Tracking. *Methods* **2017**, *115*, 80−90.
(38) Monnier, N.; Barry, Z.; Park, H. Y.; Su, K. C.; Katz, Z.; English, B. P.; Dey, A.; Pan, K.; Cheeseman, I. M.; Singer, R. H.; Bathe, M. Inferring Transient Particle Transport Dynamics in Live Cells. *Nat. Methods* **2015**, *12*, 838−840.
(39) Combet, C.; Blanchet, C.; Geourjon, C.; Deleage, G. Nps@: Network Protein Sequence Analysis. *Trends Biochem. Sci.* **2000**, *25*, 147−150.
(40) Landau, M.; Mayrose, I.; Rosenberg, Y.; Glaser, F.; Martz, E.; Pupko, T.; Ben-Tal, N. Consurf 2005: The Projection of Evolutionary Conservation Scores of Residues on Protein Structures. *Nucleic Acids Res.* **2005**, *33*, W299−302.
(41) Dosztanyi, Z.; Csizmok, V.; Tompa, P.; Simon, I. Iupred: Web Server for the Prediction of Intrinsically Unstructured Regions of Proteins Based on Estimated Energy Content. *Bioinformatics* **2005**, *21*, 3433−3434.

DOI: 10.1021/acsnano.8b02469
ACS Nano 2018, 12, 6137−6146